Article

Shock-Absorbing and Failure Mechanisms of WS and MoS Nanoparticles with Fullerene-like Structures under Shock Wave Pressure

Yan Qiu Zhu, Toshimori Sekine, Yan Hui Li, Michael W. Fay, Yi Min Zhao, C. H. Patrick Poa, Wen Xin Wang, Martin J. Roe, Paul D. Brown, Niles Fleischer, and Reshef Tenne

J. Am. Chem. Soc., **2005**, 127 (46), 16263-16272• DOI: 10.1021/ja054715j • Publication Date (Web): 01 November 2005

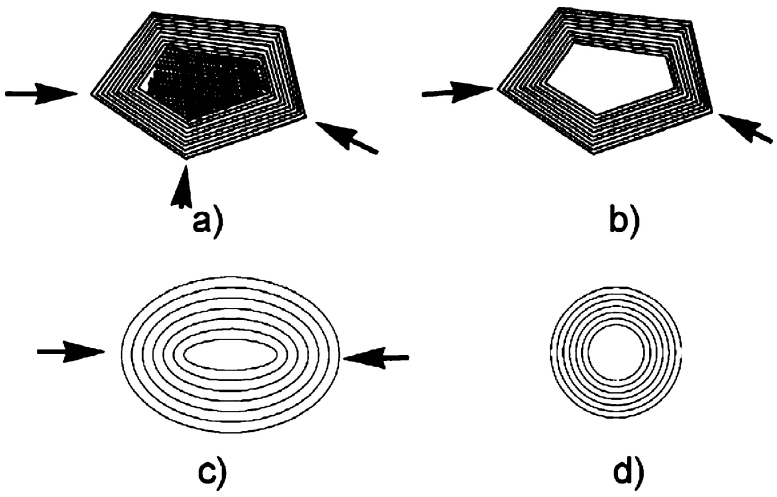

More About This Article

Additional resources and features associated with this article are available within the HTML version:

- Supporting Information
- Links to the 6 articles that cite this article, as of the time of this article download
- Access to high resolution figures
- Links to articles and content related to this article
- Copyright permission to reproduce figures and/or text from this article

View the Full Text HTML

J|A|C|S
ARTICLES
Published on Web 11/01/2005

Shock-Absorbing and Failure Mechanisms of WS_2 and MoS_2 Nanoparticles with Fullerene-like Structures under Shock Wave Pressure

Yan Qiu Zhu,*,† Toshimori Sekine,‡ Yan Hui Li,† Michael W. Fay,† Yi Min Zhao,† C. H. Patrick Poa,§ Wen Xin Wang,¶ Martin J. Roe,† Paul D. Brown,† Niles Fleischer,# and Reshef Tenne⊥

Contribution from the School of Mechanical, Materials and Manufacturing Engineering, and School of Chemistry, University of Nottingham, University Park Nottingham NG7 2RD, U.K., Advanced Materials Laboratory, National Institute for Materials Science, 1-1 Namiki, Tsukuba 305-0044, Japan, Nano-Electronics Centre, Advanced Technology Institute, Guildford, Surrey GU2 7XH, U.K., NanoMaterials, Ltd., Weizmann Science Park, 2 Holtzman Street, Rehovot 76124, Israel, and Department of Materials and Interfaces, Weizmann Institute of Science, RehoVot 76100, Israel

Received July 14, 2005; E-mail: yanqiu.zhu@nottingham.ac.uk

Abstract: The excellent shock-absorbing performance of WS_2 and MoS_2 nanoparticles with inorganic fullerene-like structures (IFs) under very high shock wave pressures of 25 GPa is described. The combined techniques of X-ray diffraction, Raman spectroscopy, X-ray photoelectron spectroscopy, thermal analysis, and transmission electron microscopy have been used to evaluate the diverse, intriguing features of shock recovered IFs, of interest for their tribological applications, thereby allowing improved understanding of their antishock behavior and structure−property relationships. Two possible failure mechanisms are proposed and discussed. The supershock-absorbing ability of the IF-WS_2 enables them to survive pressures up to 25 GPa accompanied with concurrent temperatures of up to 1000 °C without any significant structural degradation or phase change making them probably the strongest cage molecules now known.

Introduction

Inorganic fullerene-like materials (IFs) generally refer to the closed cage nanoparticles, being first used to describe the dichalcogenides of tungsten or molybdenum nanoparticles or nanotubes.[1] This concept was then extended after the successful synthesis of other new forms of layered hollow nanostructures. To date, MX_2 is widely used to represent the series of inorganic fullerene nanostructures where M = W, Mo, Nb, Ti, or Ta, and X = S, Se, or Te,[2] from their corresponding 2H polytypes, while their corresponding 3R polytypes generally lead to nonhollow nanostructures. These nanoparticles offer many valuable functional properties, one of the most extraordinary of which is the excellent lubricant behavior exhibited by IF-WS_2 and IF-MoS_2.[3] As a solid-state lubricant, they have shown superior tribological performance over traditional platelet crystal analogues, such as low coefficient of friction and low rate of wear, especially under high loads. Furthermore, porous matrixes containing such IFs exhibited lower friction and improved wear-resistant behavior.[4] The demand for IF-WS_2 is increasing, with more than 1000 ton of orders placed in 2005 alone. Therefore, once their production is scaled up within the next few years, they are expected to find major applications in the automobile, aerospace, machining, microelectronic, sport, and medical industries.[5,6] The tribological properties of these nanomaterials are intimately related to their mechanical performance. Moreover, recent investigations show that IFs can withstand collisions with 25 GPa shock waves and greater, suggesting new potential for the engineering applications for these materials.[7,8] Thus, a more thorough investigation of their diverse mechanical properties is warranted.

Of the many critical factors affecting the mechanical properties of IF nanoparticles, their initial structural and crystalline features are considered to be the most important. This includes the overall particle size, particle contour dimension, and defect

† School of Mechanical, Materials and Manufacturing Engineering, University of Nottingham.
‡ National Institute for Materials Science.
§ Advanced Technology Institute.
¶ School of Chemistry, University of Nottingham.
# NanoMaterials, Ltd.
⊥ Weizmann Institute of Science.

(1) Margulis, L.; Salitra, G.; Tenne, R.; Talianker, M. *Nature* **1993**, *365*, 113.
(2) Hershfinkel, M.; Gheber, L. A.; Volterra, V.; Hutchison, J. L.; Margulis, L.; Tenne, R. *J. Am. Chem. Soc.* **1994**, *116*, 1914.
(3) Rapoport, L.; Bilik, Y.; Feldman, Y.; Homyonfer, M.; Cohen, S. R.; Tenne, R. *Nature* **1997**, *387*, 791.
(4) Rapoport, L.; Lvovsky, M.; Lapsker, I.; Leshchinsky, V.; Volovik, Y.; Feldman, Y.; Margolin, A.; Rosentsveig, R.; Tenne, R. *Nano Lett.* **2001**, *1*, 137−140.
(5) Rapoport, L.; Feldman, Y.; Homyonfer, M.; Cohen, H.; Sloan, J.; Hutchison, J. L.; Tenne, R. *Wear* **1999**, *225*−*229*, 975.
(6) Drummond, C.; Alcantar, N. A.; Israelachvili, J.; Tenne, R.; Golan, Y. *Adv. Funct. Mater.* **2001**, *11*, 348−354.
(7) Zak, A.; Feldman, Y.; Alperovich, V.; Rosentsveig, R.; Tenne, R. *J. Am. Chem. Soc.* **2000**, *122*, 11108.
(8) Golan, Y.; Drummond, C.; Homyonfer, M.; Tenne, R.; Israelachvili, J. *Adv. Mater.* **1999**, *11*, 934.

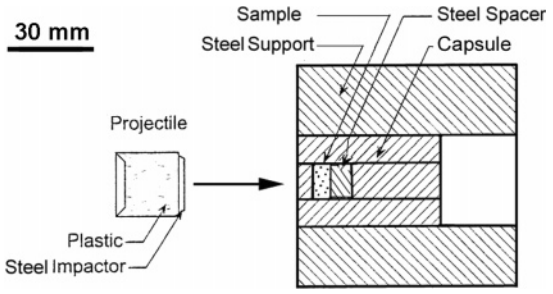

Figure 1. Shock wave recovery sample assembly for a single-stage gun experiment.

intensities within the nanocrystals. In particular, when used as solid-state lubricants, the external loads will generate highly dynamic compressive and tensile forces in response to the severe pressures and shear stresses applied to the IF nanoparticles. Thus, the relationships between the original structures and the applied pressures are quite important and should be assessed.[8] In this context, it becomes appropriate to compare the lubrication process with that of dynamic compression, in view of the nonperiodic compression and sliding arising from the conversion of dynamic pressure to applied shear stress.

Extremely high pressures can induce shear forces leading to crystal deformation, e.g., with resultant phase changes among various polytypes[9] and even the formation of new crystalline phases.[10] For the case of uniaxial hydrostatic compression, the particles normally experience deformation forces over a relatively long period of time, while the application of nonuniaxial dynamic pressures can lead to very severe transient shear stresses, inducing more extensive levels of structural deformation in a matter of microseconds.[11] The latter situation more closely resembles the actual process of dynamic tribology.

In this paper, nonuniaxial high pressures are applied to WS_2 and MoS_2 IFs, via a series of shock recovery experiments, to profile the process of IF response and deformation. The detailed structural features defining postshock samples, subjected to various pressures, are described with reference to X-ray diffraction (XRD) and transmission electron microscopy (TEM) investigations. The results reveal that the IF cages are excellent shock absorbers, withstanding shock pressures up to 25 GPa at light destruction. The reasons for the ability of the IF cages to sustain such high pressures are discussed. The mechanism for the structural failure of IFs at pressures exceeding the allowed pressures is discussed. This study shows that the structural and chemical integrity of the nanoparticles is mostly preserved under such high loads; thereafter, they collapse and become gradually destroyed by exfoliation and thermal decomposition.

Experimental Section

The shock recovery experiments were carried out at the National Institute for Materials Science (NIMS), Tsukuba, Japan, using a 10-m-long single-stage powdered gun, being versatile equipment for dynamic high-pressure physics, chemistry, and materials science research.[11] The experimental arrangement is illustrated in Figure 1. For a specified amount of powder, a pellet speed, ranging from 0.5 to 2 km s^{-1}, as measured by the flying magnet method, could be repeatedly achieved, generating impact shock pressures from a few GPa up to a few tens of GPa.

The starting IF powdered materials, supplied by NanoMaterials Ltd., were initially pressed into a cylindrical stainless steel (SUS304) sample container (200 mg/sample). A constant pressure, using a 200 kg load, was applied during sample compaction to achieve comparable sample densities. The resulting sample disks were $\varnothing 12 \times 0.5$ mm in size, with an average density of 3.90 g/cm^3, as compared with the bulk 2H-WS_2 crystal density of 7.6 g/cm^3.

After the shock wave experiments, the deformed stainless steel sample containers were sectioned using a lathe and the postshock powders then carefully recovered using a scalpel. Roughly a 5−10% increase in the diameter of the sample containers occurred under shock compression, with a corresponding reduction in the container height. It was difficult to measure the average density of the postshock samples. It was assumed that the shock press did not lead to a significant change in the sample densities, particularly after the sample pressures were released. Indeed, the recovered samples appeared identical to the starting powder in color, with the exception of some larger compacted volumes for samples subjected to very high pressures; however, these volumes easily broke up into isolated nanoparticles during subsequent sonication in acetone. Accordingly, hardly any sintering effects occurred as a consequence of the concurrent temperature rise associated with the shock press. Table 1 summarizes the starting materials, shock pressures applied, and the overall degree of damage exhibited by the samples, as assessed using XRD and TEM.

CM-200 and Joel-4000fx high-resolution transmission electron microscopy (operated at 200 and 400 kV, respectively), XPS, thermal analysis, Raman spectroscopy, and powder X-ray diffractions were employed to characterize the detailed structural features of the recovered postshock samples. Sample crystal structures were appraised using a Siemens D500 X-ray diffractometer operating at 40 mA/40 kV, to produce Cu Kα radiation, with a scanning rate of 0.02 deg/min.

A VG Scientific Escalab Mark II X-ray photoelectron spectrometer (XPS) was employed to analyze the surface integrity of the samples, using nonmonochromated Al Kα X-rays, operated at an anode potential of 10 kV and a filament emission current of 20 mA. The electron spectrometer comprised a hemispherical analyzer and was operated in a constant energy mode (CAE) at electron pass energies of 50 and 10 eV for survey scans and the high-resolution peak scans, respectively. The high vacuum in the analysis chamber was typically better than 4×10^{-9} mbar. The electron takeoff angle used was 90° and the area of converted power analyzed approximately 1 cm × 1 cm. A survey scan spectrum in the 0−1100 eV binding energy (BE) range was collected for each sample in addition to high-resolution scans from individual peaks of interest. A Shirley reduction model was used to subtract the background, and individual peaks were fitted at a Gauss/Lorenz ratio of 70/30. Background removal, peak fitting, and peak area determination were performed using the CasaXPS software. Semiquantitative analyses (i.e., atomic % determination) of the survey spectra were performed using modified Scofield elemental sensitivity factors.

An SDT Q600 system was used for the sample thermal gravimetric analysis (TGA), with a compressed air flow rate of 100 sccm, with an isothermal held at 50 °C, and ramp up to 600 °C at 10°C/min, followed by natural cooling.

Results and Discussion

A. Brief Description of Shock Wave Experiments. Although the general features of the shock recovery experiments are initially described, a brief description of their main features is warranted in order to achieve a better understanding of the following results and discussions. When a high-speed projectile hits a sample container, shock waves transmit to and propagate within the sample, inducing high shock wave pressures and extremely high temperature rises for certain samples, with almost

(9) Zhu, Y. Q.; Sekine, T.; Kobayashi, T.; Takazawa, E. *J. Mater Sci.* **1998**, *33*, 5883.
(10) Zhu, Y. Q.; Sekine, T.; Kobayashi, T.; Takazawa, E.; Terrones, M.; Terrones, H. *Chem. Phys. Lett.* **1998**, *287*, 689.
(11) Horie, Y.; Sawaoka, A. *Compression Chemistry of Materials*; KTK Scientific Publ.: Tokyo, 1993.

Table 1. Summary of the Shock Recovery Experiments: XRD Data and the Damage Assessed

materials	shock pressures (GPa)	XRD measured 2θ for (002)/deg	d_{002} (nm)	fwhm (deg)	calculated layer thickness (nm)	TEM assessed degree of damage
pristine IF-WS_2	n/a	14.262	0.6205	0.619	12.93	
	9.74	14.264	0.6203	0.604	13.25	lowest
	20.4	14.324	0.6182	0.592	13.52	lower
IF-WS_2	21.2	14.326	0.6182			low
	21.7	14.349	0.6141	0.59	13.56	low
	23.6	14.352	0.6111	0.58	13.80	moderate
	30.8	14.519	0.6084	0.367	21.82	very high
	35.6					destroyed
IF-MoS_2	24.6	14.350	0.612			lower

no obvious movement or positional change. It is noted that the sharp temperature rise generated concurrently by the shock waves will be strongly affected by the sample density; this was not a primary consideration of this investigation since the sample densities remained constant. While the shock wave reverberation does not last longer than a few microseconds, the decay of the thermal spike lasts longer due to the limited thermal diffusivity of the sample. This is an important consideration when accounting for the chemical processes that take place, especially under high pressures (>20 GPa), where the temperature may rise to 1000 °C. For a porous particulate sample, the passage of the shock wave front will generally cause particle, pore collisions and a minor condensation in volume. The ∅28 mm projectiles used in this study produced a fairly uniform pressure distribution across the sample containers of diameter ∅12 mm. Accordingly, the averaged pressure, calculated using a speed impendent measurement based on the flying magnet method,[11] is considered to be equivalent across all the individual particles.

Even though it is not easy to obtain an accurate value for the temperature attained during shock due to the lack of specific physical data for the IF cages, the temperature rises immediately after the first passage of the shock wave may be estimated from a consideration of nonporous WS_2, assuming that the Hugoniot of solid WS_2, with a density of 7.6 g/cm^3, is approximated by solid W plus S_2 and that the solid WS_2 is compressed by a single shock process.[11] Accordingly, temperature increases of 700 and 2100 °C were estimated, under induced pressures of 15 and 30 GPa, respectively. In this context, the presence of porosity (related to a lowering of density) of the samples will be associated with a higher temperature rise, while shock wave reverberation would lead to the dissipation of energy, in turn being associated with a lower associated temperature rise. Bulk WS_2 is unstable above 1400 °C and decomposes to its elements. The bulk form is somewhat more stable than the IF nanoparticles,[12] but the particle size and rate of heating need to be taken into account. This very rough temperature approximation, combined with the TEM verification of no melting or sintering among the IFs, indicates that the temperature increases associated with the current experiments must have been below the decomposition temperature, estimated at a level of ca. 1000 °C under induced conditions of 20−25 GPa. The temperature rise accentuated by porosity is considered to induce the highest temperatures at the near surface of the solid particles, helping to explain the sulfide−oxide conversion observed limited to the top few layers at the particle surfaces. This surface oxidation phenomenon will also be dependent on the diffusivity/reactivity of oxygen under these experimental conditions.

B. Overall Features. B.1. X-ray Diffraction. XRD spectra for the postshock samples are presented in Figure 2, indicating an overall minor change of structural integrity when compared with that of the starting material. All the primary diffraction peaks from the spectrum of the starting powder (Figure 2a) are reproduced within the spectra of the postshock samples, but with few significant intensity variations, particularly at higher diffraction angles, as the shock wave pressure increases. Further, there is a small shift of the 002 diffraction peak values with increasing pressure, as summarized in Table 1. Single-crystal Co powder was employed as an internal standard during related diffraction experiments to minimize systematic errors.

The d_{002} spacing for the postshock IFs was reduced by <0.5% at 9.73 GPa and up to 2% at 30.8 GPa, corresponding to $d_{002} =$ 0.608 nm, as compared with the initial value of $d_{002} = 0.62$ nm. It is known that small (very much less than micrometer-sized) IF particles, exhibit an average {002} layer separation slightly larger than that of the corresponding platelet particles[2,12] due to the stress release mechanism of folded layers which introduces various defects into the IF structures and leads to an expansion of the interlayer spacing. Conversely, the {002} interlayer separation in larger (close to micrometer-sized) IF particles is reduced, being even smaller than that of their 2H platelet counterparts, because of the increased strain the inner layers suffer in response to inward compressions toward the central hole from the outer shells.[13] A similar stress leads to the diamond conversion from inner shell/cores of carbon nano-onions induced by such structural compressive strains.[14] Since the preshock and postshock sample particle sizes examined here are all well under the micrometer range (as will be discussed later), there is an expectation for them to exhibit slightly larger d_{002} spacings as compared with those of the bulk.

For the case of bulk crystalline samples, shock wave pressures generally cause severe lattice distortions, defects, and the expansion of interlayer spacings arising from crystal deformation,[11] while the present XRD study confirms a reduction in d_{002} with increasing pressures. However, it is noted that caged and hollow IFs are structurally different from platelet crystalline powders, and hence it is expected that they exhibit dissimilar responses to shock waves, even when defects have been induced within the layers.

The 002, 004, and 006 diffraction intensities became significantly enhanced as the shock pressures increases, as compared

(12) Hacohen, Y. R.; Biro, R. P.; Prior, Y.; Gemming, S.; Seifert, G.; Tenne, R. *Phys. Chem. Chem. Phys.* **2003**, *5*, 1644.

(13) Remskar, M.; Mrzel, A. *Curr. Opin. Solid State Mater. Sci.* **2004**, *8*, 121.
(14) Banhart, F.; Ajayan, P. M. *Nature* **1996**, *382*, 433.

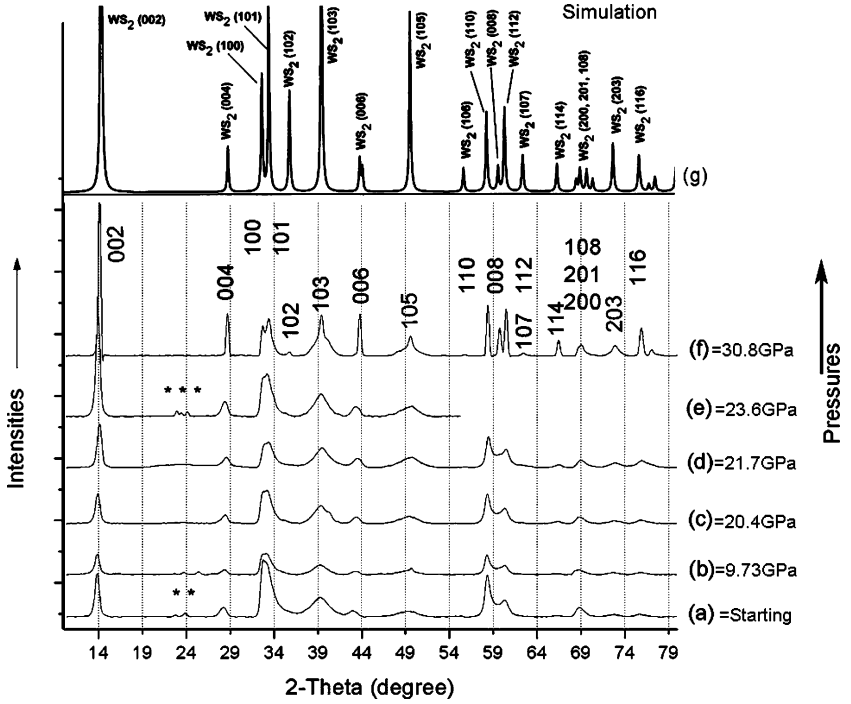

Figure 2. X-ray diffraction profiles of IF-WS_2. Pressure increases from bottom (starting IFs, from line a to line f) (30.8 GPa). Patterns b−e correspond to pressures of 9.73, 20.4, 21.7, and 23.6 GPa, respectively. Peaks marked with an asterisk (∗) at ca. 24° are the unconverted WO_x phases wrapped by the IFs, possibly $W_{18}O_{49}$. (g) A simulation pattern for WS_2 nanoparticles at ambient pressure.

with the 100 and 101 intensities, indicating that the layered aspect of the IFs had been improved gradually. In this respect, an impact with shock waves may induce some deformation of the IF nanoparticles from a quasi-spherical into an ovoid shape, leading to enhancement of the 00*l* peaks. At ca. 10 GPa (Figure 2b), there is very little structural difference from the starting material. Below ca. 25 GPa (Figure 2c−e), only slight increased changes are observed, while at 30.8 GPa (Figure 2f), the XRD profile is very close to that of bulk 2H-WS_2 crystals,[15] Figure 2g, commensurate with the majority of IFs being collapsed at this pressure. In particular, the splitting of the 100 and 101 diffraction peaks in Figure 2f demonstrates the in-plane crystalline feature being increased substantially at 30.8 GPa. The increased extent of in-plane crystallinity indicated by the splitting of the 100 and 101 peaks, as well as the hugely enhanced 00*l* ratio reflecting the improved interlayer structure integrity and flattering of the sample shape, are the symptomatic of the loss of the quasi-spherical cagelike structures at 30.8 GPa. In view of the resemblance of the XRD profiles of Figure 2a−e, these results indicate that caged WS_2 samples are able to sustain applied pressures of up to 25 GPa.[16]

Due to the reduction in the 002 diffraction spacing, it might be envisaged that the overall particle size of the postshock samples should shrink accordingly. However, careful comparison of full width at half-maximum (fwhm) values for the d_{002} peaks, following use of Sherrer's equation, suggests an increase in the sizes of postshock particles. The d_{002} fwhm values and the calculated (002) layer thickness changes are summarized in Table 1. The pressure versus crystal size relationship can then be obtained, Figure 3. A minor change in crystallite size

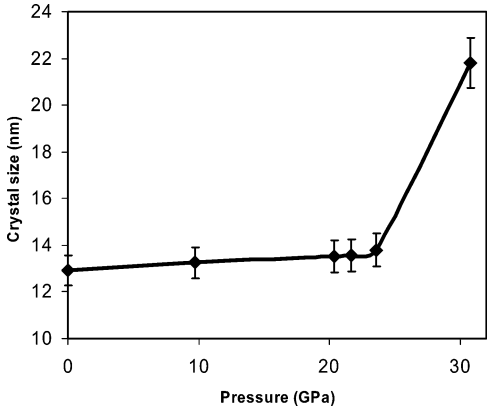

Figure 3. Estimated crystal sizes of postshock IF-WS_2 varying with applied pressures, with a 5% error.

was observed when the shock pressure was low (9.73 GPa), being comparable to that of the starting IF-WS_2, with a slight increasing change over 20 GPa followed by a significant coarsening of the particle wall thickness when the applied shock pressure exceeded 30 GPa. The increase in particle size correlates with the reduction in-plane spacing.

Shock-induced defects would not be responsible for such an apparent overall increase in particle size. The slight increase in the crystallite size of samples subjected to pressures in the range of 20−25 GPa is hence considered to originate from a combination of interlayer spacing reduction and the progressive collapse of some of the IF particles, leading to an increase in the projected area of the particles. This collapse would lead to an increase of the XRD 00*l* intensities for two reasons. First, some of the IF nanoparticles are crushed and converted into platelets. Second, one collapsed IF tube/sphere may form several flat flakes.[15] This explanation agrees well with the following Raman and TEM analyses in that the IF particles are fairly stable

(15) Zhu, Y. Q.; Sekine, T.; Brigatti, K. S.; Firth, S.; Tenne, R.; Rosentsveig, R.; Kroto, H. W.; Walton, D. R. M. *J. Am. Chem. Soc.* **2003**, *125*, 1329.
(16) Zhu, Y. Q.; Sekine, T.; Li, Y. H.; Wang, W. X.; Fay, M. W.; Edwards, H.; Brown, P. D.; Fleischer, N.; Tenne, R. *Adv. Mater.* **2005**, *17*, 1500.

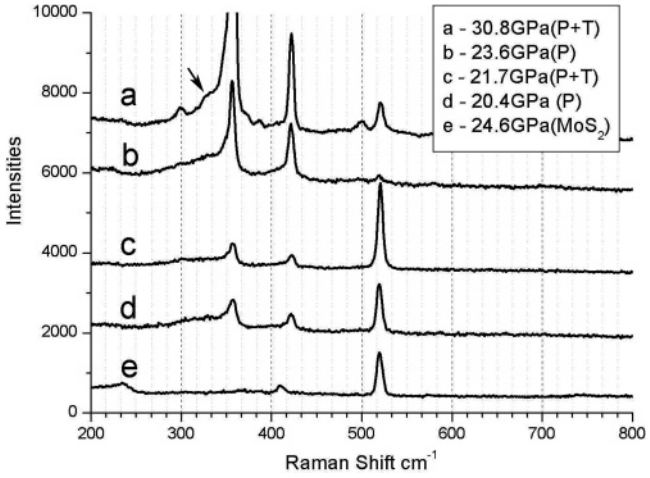

Figure 4. Raman spectra of samples subject to pressures as marked. Profile e is for IF-MoS_2. The peak at 521 cm^{-1} arises from the Si substrate.

under shock pressures of ~25 GPa, resulting in minimal destruction only. The significant enlargement in particle wall thickness (> 60% increase compared to that of the original IFs) for samples subjected to shock waves above 30 GPa suggests once again that the particles are more strongly flattened and crushed flakes are laid together. This phenomenon is amplified by the concurrent high temperatures, leading to a softening of the quasi-spherical structures. This indicates that ~25 GPa is the maximum allowed shock pressure load for IF-WS_2 before the structure of the particles is destructed. The Young's modulus of MoS_2 is 40% higher than that of WS_2 suggesting that IF-MoS_2 nanoparticles could sustain shock wave pressure as high as 30 GPa, as indeed is observed in a preliminary study.[17]

B.2. Raman Analysis. A Raman structural study was also performed to reveal the general shock wave effects on the vibration response of the cagelike IF samples. Attention was given to WS_2 samples under an applied pressure of ~20 to 30 GPa, compared with starting IF material, bulk 2H platelet WS_2 powder, and MoS_2 powder. A few spectral peak position and intensity changes were observed for the examined samples, while certain frequencies remained identical to the spectra of the starting material and 2H platelet particles (Figure 4).

It has previously been reported that the 323 cm^{-1} band in the 514.5 nm excitation spectrum of starting WS_2 nanotubes broadens to a shoulder in the spectrum of nanotubes shocked under conditions of 21 GPa.[15] The band at 323 cm^{-1} also appeared as a shoulder in the spectra of both shocked and unshocked samples excited with 632.8 nm radiation. Under all tested pressures, using 735 nm laser excitation, the spectra of the IF nanoparticles also showed a broadening of the 323 cm^{-1} to a shoulder (Figure 4, arrowed), becoming accentuated with increasing pressure. These spectra suggest there were no significant changes to the overall structure of the WS_2 samples after shock, emphasizing the similarity of the local symmetry of WS_2 nanotubes and WS_2 IF spheres.

However, significant intensity increases were detected for Raman bands at 356 and 420 cm^{-1} (Figure 4a−d), corresponding to the 2H-WS_2 E^1_{2g} and A_{1g} modes, respectively, when the pressure increased from 20.4 to 30.8 GPa. Such intensity changes indicate a larger contribution of the 2H structural motif of the IF nanoparticles to the Raman response, upon increase of the applied shock wave pressure. Negligible changes in the spectra were apparent for shocked samples under 21.7 GPa, as compared with that of the starting powder, while an obvious intensity increase of the 356 cm^{-1} band was associated with pressures exceeding 23.6 GPa. For example, at 30.8 GPa, this peak became several times stronger than the others. In agreement with the XRD data, the IF samples subjected to 30.8 GPa shock wave pressures strongly resemble the 2H-WS_2 platelet particles, while the dominant Raman features of IF-WS_2 were barely retained.

Figure 4e shows a spectrum from IF-MoS_2 particles shocked under conditions of 24.6 GPa, indicating that little change has occurred as compared with the starting material. This is a strong indication of the superior antishock wave performance of IF-MoS_2 as compared with that of IF-WS_2. Unfortunately, the available amounts of IF-MoS_2 samples were not sufficient for conducting a series of detailed shock wave recovery tests, and consequently no comprehensive results about its ability to sustain the shock wave could be derived. At present, it is not possible to conclude whether the improved antishock behavior of IF-MoS_2 arises from a compositional difference or from the smaller size of MoS_2 nanoparticles investigated (ca. 80 nm in diameter) as compared with the analogous WS_2 (ca. 150 nm in diameter). However, it is noted that the Young's modulus of bulk 2H MoS_2 (240 MPa) is slightly higher than that of bulk 2H-WS_2 (150 MPa), which would favor the improved resistance to shock of MoS_2.

B.3. XPS Spectra. The structural investigations reported so far have confirmed that the dominant products of IF-WS_2 and IF-MoS_2 are retained within the postshock samples, respectively. The high temperatures produced concurrently with the shock pressures may potentially affect both the crystal structure and the chemical composition of the recovered samples, and this consideration has been omitted from previous discussions.[15,16] The potential decomposition or chemical reaction of the IF nanoparticles with trapped oxygen is likely to be limited to the topmost atomic layer, being dynamically constrained from further penetration toward the inner core.[13]

XPS investigation indicated a maximum of 2.4 atom % increase with W_{4f} (WO_3) signal at the expense of a 2.4 atom % reduction for the W_{4f} (WS_2) signal, for samples subjected to 23.6 GPa, as compared with the starting material (Figure 5). In view of the estimated temperature rise of ~1000 °C, over a very short time frame, it is suggested that the outer shell of the IF-WS_2 particles has reacted with oxygen trapped inside the sample container, leading to superficial WO_3 formation by replacing the outermost atomic layers of the IF-WS_2 structures. The limited oxidation of the outer sample surfaces exposed to such transient peak temperatures (~1000 °C) is in keeping with TGA data (see the next section).

Even though WS_2 are gradually oxidized at temperature above 400 °C,[12,13] during the brief temperature spikes induced by the shock waves, IF-WS_2 particles are dynamically capable of sustaining much higher temperatures, accompanied by high pressures. The minute level of superficial oxide formed during the shock test does not contribute significantly nor consistently to the XRD data. The two occasionally observed oxide peaks (Figure 2, denoted ∗) are considered to originate from unconverted WO_x cores sheathed within the WS_2 layers (Figure 10),

(17) Kaplan-Ashiri, I.; Cohen, S. R.; Gartsman, K.; Rosentsveig, R.; Seifert, G.; Tenne, R. *J. Mater. Res.* **2004**, *19*, 454.

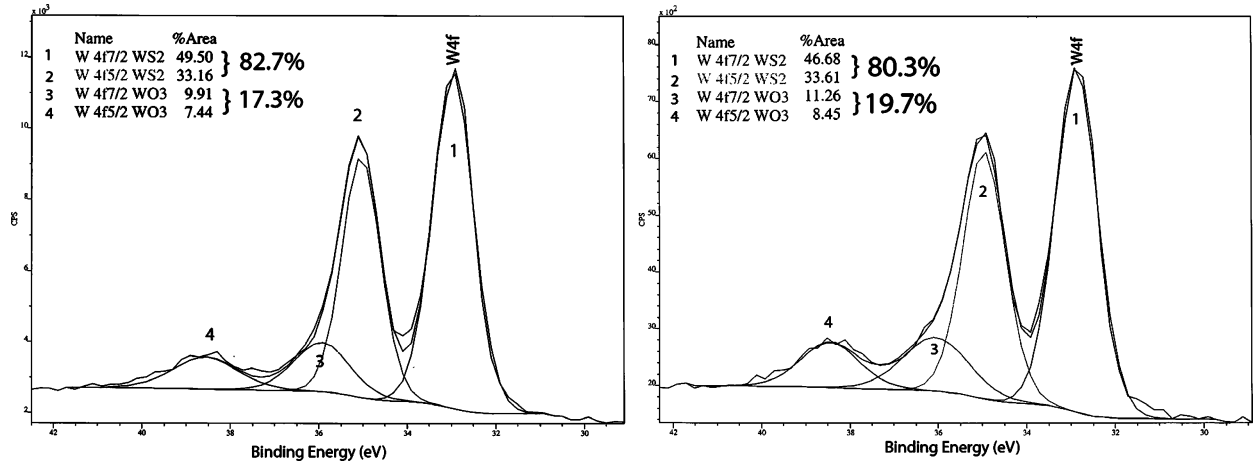

Figure 5. XPS profiles of original IF-WS_2 and the postshock IF-WS2 (right, 23.6 GPa) samples, showing the increases of their oxide content.

with no conclusive evidence from XRD indicating an overall increase in surface oxide content for the postshock samples. The investigation from XPS for a slight change (2.4 atom %) from W_{4f} (WS_2) to W_{4f} (WO_3) is attributed to a slight change in oxide content at the particle surface. It cannot be ruled-out, however, that the superficial oxide which was observed by the XPS of shocked samples is amorphous; hence it would not, in any event, be revealed by XRD measurement.

XPS measurements were similarly employed to study the wear performance of IF-WS_2 nanoparticles by Rapoport et al.[4] Under a very light load of less than 150 Nm/s, IF-WS_2 nanoparticles dispersed in oil during friction and wear experiments were found to exhibit superior antioxidation performance as compared with their counterpart 2H platelet crystals. The propensity for restrained oxidation, in general terms, reflects the material limited reactivity and confirms its structural stability. For MoS_2 samples under 24.6 GPa, the XPS results suggested only a negligible reduction in the Mo surface intensity, as compared with the unshocked IF-MoS_2 signal.

The relative stability of IF materials vis a vis their bulk products is determined not only by the thermodynamics but also through the kinetics of the relevant reaction. Globally, thermodynamic considerations, supported by first principle ab initio calculations,[18] indicate that bulk phases are somewhat more stable than the analogous IF nanoparticles. Notwithstanding this observation, the reactivity of the IF phases with respect to oxidation or reaction with water is found to be slower than that of the bulk material.[12] 2H-MS_2 platelets expose their prismatic $\{hk0\}$ planes to the atmosphere, promoting fast diffusion of oxidants into the interlayer van der Waals gaps. Conversely, the closed nature of IF cages poses a kinetic barrier to the process of diffusion, and consequently the oxidation reaction is slowed. This observation explains that the reactivity of IF nanoparticles with respect to oxidation is determined to a large extent by the morphology and the perfections of their structures. Generally, the smaller the IF nanoparticles, the higher the built-in elastic strain and the more reactive they are expected to become.[12]

In this context, the average size of the IF-MoS_2 nanoparticles exhibited (80 nm) is smaller than that of the IF-WS_2 nanoparticles (140 nm). Therefore, under similar shock conditions of pressures and presumably comparable rise in temperatures, taking size considerations alone, the smaller IF-MoS_2 particles might be expected to be more reactive than IF-WS_2, leading to severer oxidation. However, the XPS results of the nanoparticles which sustained shock waves showed that less surface oxidation had occurred for the IF-MoS_2 (<0.5 atom %) as compared to IF-WS_2 (2.4 atom %) under similar conditions. Therefore, it is suggested that the higher resistance to oxidation exhibited by the IF-MoS_2 as compared to that of IF-WS_2 stems mainly from its more perfect spherical shape, rather than its smaller size. As a consequence, this will also contribute to the superior antishock behavior of IF-MoS_2 as compared with that of IF-WS_2.

B.4. Thermal Analysis. Different shock pressures are expected to generate varying degrees of damage within IF samples. The higher the pressure applied, above a certain threshold, the more defects would be likely to result. This is emphasized by a broadening of the100 and 101 XRD peaks with increasing pressure (Figure 2). Such defective sites, with higher associated surface energy, might be expected to make the postshock samples more susceptible to oxidation.

Accordingly, TGA was applied to ascertain the overall structural damage induced under different shock wave pressures. Figure 6 presents the TGA results, comparing the response of starting IF nanoparticles to those shocked under pressures of 9.7 and 23.6 GPa, respectively. A substantial increase in the threshold temperature for the onset oxidation of the postshock samples, i.e., 416 °C at 9.7 GPa and 418 °C at 23.6 GPa was identified as compared with a value of 389 °C for the preshock IF-WS_2 (Figure 6, joint of the vertical line and the top horizontal line), in agreement with a recent report by Schufferhauer et al.[18]

The samples exposed to air during TGA for the purpose of oxidation might be expected to induce a combination of contradicting effects, which cannot be easily reconciled. On one hand is the higher the defect density, and consequently the lower the starting oxidation temperature. However, both XRD and Raman analyses suggest that the higher is the pressure—in particular when the shock pressures exceed 30 GPa which is combined with high temperatures—the more IF-WS_2 is being converted to well-crystallized 2H platelets. It was established that 2H platelets a few micrometers in size oxidize at somewhat higher temperatures than the IF nanoparticle analogues,[12] particularly under slow temperature ramp. On the other hand, the concurrent temperatures that were produced by the impact

(18) Schufferhauer, C.; Wildermuth, G.; Felsche, J.; Tenne, R. *Phys. Chem. Chem. Phys.* **2004**, *6*, 3991.

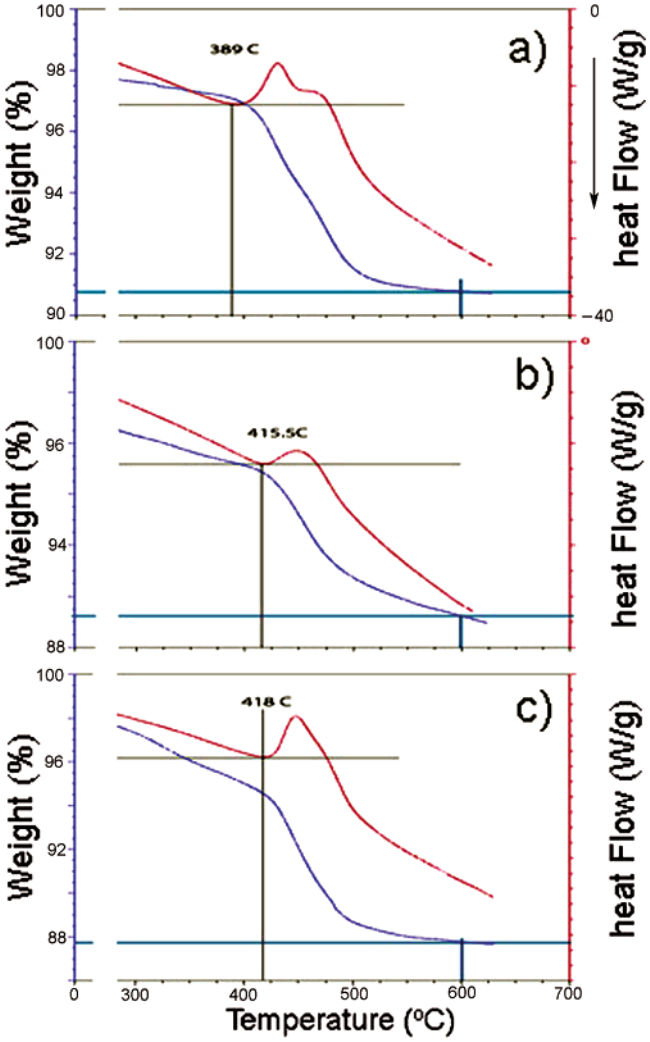

Figure 6. Thermal analyses of IF-WS_2 samples: (a) pristine materials, (b) 9.7 GPa, and (c) 23.6 GPa. The onset oxidation temperatures (junction of the horizontal and vertical lines) are determined by the sudden heat flow increase (right). The dropping line in the figures shows the weight loss.

of the shock waves with the sample may have led to the formation of an overlayer of oxide on top of each IF nanoparticle, as confirmed by the above XPS analyses. The outer oxide shells would inevitably hinder the inner IF shell from further oxidation by limiting oxygen diffusion, thus raising the onset oxidation temperature, as the oxidation process is believed to occur from outside inward.[13] Therefore, it was expected that the results of the TGA analysis will be influenced by a combination of complex and counteracting effects.

These results shown in Figure 6 indicate that, following the application of comparatively modest pressures through which no transformation to 2H structures are possibly involved, the significant rise in the temperature for the onset of oxidation of the postshock samples must have resulted primarily from the superficial oxide layers and thus subsequently the removal of dangling bonds caused by the pressure and temperature induced during shock. The difference of the onset oxidation temperature for the two postshock samples is very small, suggesting that any defects induced within the IFs are not particularly extensive under such shock conditions. Hence, the dominant effect revealed here seems to be the slight oxidation of the outmost IF particle surfaces as a result of the rapid rise in temperature associated with the shock wave. The shock-absorbing abilities

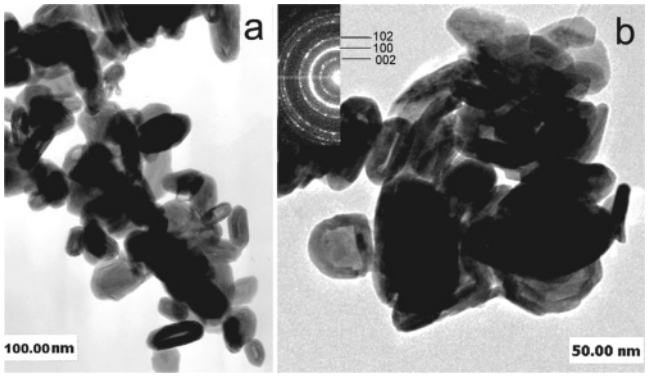

Figure 7. TEM images of (a) the pristine IF-WS_2 and (b) the postshock WS_2 at 23.6 GPa. The inset in (b) is the corresponding ED image of the particles, showing the 002 diffraction ring.

of the IF-WS_2 nanoparticles enable them to survive pressures up to 25 GPa without apparent substantial increase in their defect densities, while slight surface oxidation originated from the concurrent high temperatures associated with the shock waves, in turn, contribute to the upshift of the onset oxidation point, observed during DTA investigation.

B.5. TEM Investigation. The morphology of the starting IF-WS_2 particles is illustrated by Figure 7a, consisting mainly of hollow polyhedral structures with quasi-spherical, or more often, ovoid shapes, some of which contain WO_x cores. The presence of a remnant oxide core suggests that the synthesis had not gone to completion, possibly because these nanoparticles were introduced into the reactor during the later stages of synthesis. The size distribution of the particles is fairly uniform, ranging from 100 to 150 nm.

Although these IF-WS_2 structures are termed inorganic fullerenes, their morphology is only slightly reminiscent of the perfect C_{60} cages in terms of their nested structures. Generally, it is considered that the pronounced polyhedral features of the particles will have a complex effect on their property.[19] The typical shocked particles under conditions of ~25 GPa are shown in Figure 7b, indicating that the particulate structures are very similar to those of the starting powder. Selected area electron diffraction (SAED) patterns (Figure 7b, inset) averaging over many nanoparticles confirm the dominant presence of IF-WS_2, in accordance with the XRD data.

B.6. Corner Effects. Figure 8a−d shows a series of HRTEM images across a partly damaged small IF-WS_2 particle (Figure 8e), illustrating the most distinctive characteristics observed under shock wave pressure above 20 GPa. Regions (a) and (c) are illustrative of broken WS_2 layer connections, while regions (b) and (d) are representative of intact WS_2. Clues to the response of such a particle under extreme shock waves arise from the remnant particle. By extending the residual layers, it might be possible to infer the shape of the original particle (Figure 8f), possibly with sharp tips at the top and bottom corners. The inference is that sharp tips at the particle corners were broken under the applied shock pressures and possibly removed thereafter during sample preparation under sonication in acetone. The suggestion is that remnant smooth edges (Figure 8d) represent regions with a more uniform stress distribution, being capable of sustaining much higher shock pressures.

(19) Frey, G. L.; Tenne, R.; Matthews, M. J.; Dresselhaus, M. S.; Dresselhaus, G. *Phys. Rev. B* **1999**, *60*, 2883.

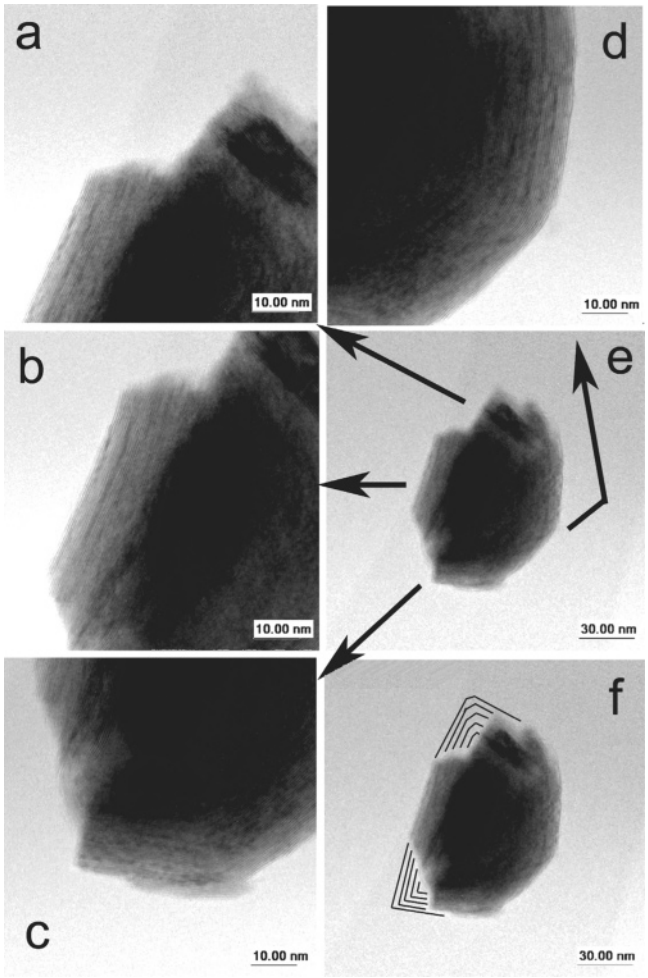

Figure 8. Series of HRTEM images from (a−e) shows the actual damages at various parts of a particle owing to different local constructions, possibly from a particle as shown in (f). Individually enlarged pictures are arrowed.

Figure 9, parts a and b, illustrates two typical IF particles that have suffered minor damage under an applied pressure of 21.6 GPa. Damage has been sustained at both the top and the bottom sharp tips of Figure 9a (arrowed), but in a different manner. For example, at the top corner, some layers had simply broken and peeled off the body, although no obvious surface oxide layer residue was observed. Parts of the original layers have disappeared from the region at the bottom of the particle (arrowed), being associated with a cone-shaped feature and a diffused zone, possibly being a tungsten oxide residue. This indicates that more than one mechanism must have been associated with the particle damage, even though both signatories result from a mortification of sharp-tipped features. The suggestion is that the latter type of modification arises from a diffusion-induced structural conversion, from sulfide to oxide, also implicated in Figure 9b, while the former type of deformation the demolition of the top part of the nanoparticle was caused mainly by pressure-induced shattering (Figure 9c). The sharp angled corners (<90 °) of polyhedral particles are more likely to sustain damage due to the enhanced localized stress concentrations, while smoother corners will survive the equivalent shock wave pressures. Hence, IF nanostructures more spherical in shape are likely to exhibit greater potential for sustaining high shock pressures, as illustrated by Figure 9d, corresponding to a particle under 24.6 GPa.

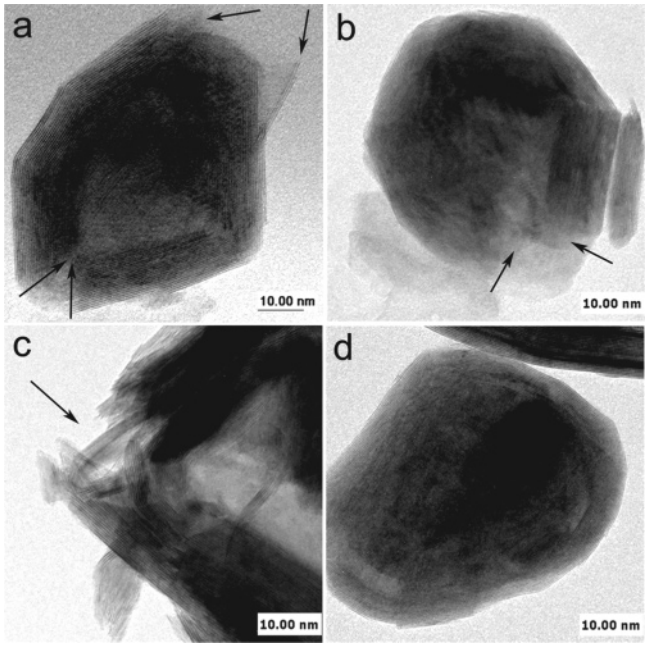

Figure 9. HRTEM images of postshock IF particles, exhibiting two typical ways of destruction. (a) Minor damages at top and bottom. Note the layers peeled up at the right and the V-shaped oxide at the bottom; (b) a V-shaped damage at the sharp corner at the bottom. Note the flake attaching to the right section. Both (a) and (b) are under 21.7 GPa; (c) Another type of partly destructed sharp angle corner, via breaking outer layers, pressure 23.6 GPa; (d) a perfectly preserved IF-MoS_2 survived 24.6 GPa, no apparent sharp corners.

The fine scale structural defects contained within IF polyhedral particles are known to be complicated.[12,19,20] They may be classified as either uniformly distributed bending defects in the vicinity of strongly arced regions of the particles or an uneven arrangement of multiple planar defects outlining sharp-tipped corners.[20] It is considered that the defect density becomes higher when the radius of the corner gets sharper, leading to sites approaching a state of unstable high energy. Under conditions of concurrent high pressure and temperature, these unstable sites are likely to undergo phase or structural changes to reduce the overall internal energy of the nanostructure in advance of catastrophic damage. The estimated shock-induced temperatures are below the chemical decomposition point of IF-WS_2, but well above the point for the onset of oxidation as indicated by the thermal property investigations,[18] and hence initial surface oxidation is highly probable. If the local temperature is high enough, and in the presence of residual oxygen and water during sample impact, it is considered that sharp tip sites will preferentially undergo oxidation, gradually replacing local WS_2 layers with tungsten oxide. Under ambient conditions, during oxidation process using oxygen and residual water, it is necessary to consider the sulfurization process which would repair the previous WS_2 structures. However, under high shock wave pressures, it is unlikely for S atoms to repair the WS_2 by replacing the already converted WO_x, due to the larger atomic size of S as compared with that of O. Furthermore, under high temperature during shock, oxidation from WS_2 is preferred, according to above DTA data.

Owing to the extremely quick increase and decrease of the temperature as a consequence of shock and the fast consumption

(20) Seifert, G.; Kohler, T.; Tenne, R. *J. Phys. Chem. B* **2002**, *106*, 2497.

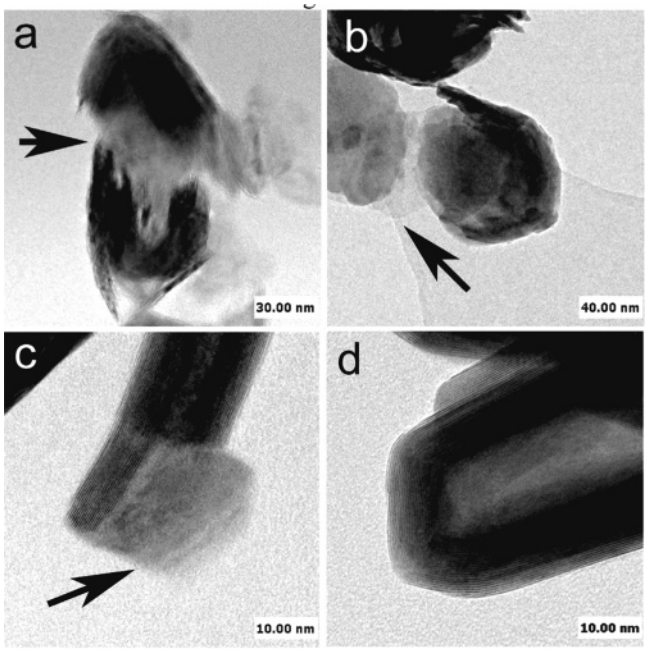

Figure 10. HRTEM images of an isolated postshock IF sample. (a) A fully broken IF-WS_2 nanoparticle with its inner WO_x core being crushed out and left to the right. The remaining top and bottom halves do not match with each other (the top one is obviously larger than the bottom one), revealing the springlike responses during stress relaxation. Pressure: 21.7 GPa. (b) A broken particle with its central oxide core being squeezed out and left to the left. (c) An end of a damaged nanotube. The residue of the inner oxide was extruded and exposed to the right. Pressure: 25.6 GPa. (d) A MoS_2 particle, undamaged. Pressure: 24.6 GPa.

of the limited amount of available trapped oxygen, possibly being associated with more highly defective sites, it is envisaged that the substitution reaction only penetrates into very restricted parts of the particles, with HRTEM observations suggesting the oxidation of regions to less than 10 nm below the particle surfaces. The reaction is controlled by the atomic diffusion distance; thus, IF-WS_2 nanostructure mortification is considered to be diffusion-controlled, leading to the development of cone-shaped oxide residues at cone-shaped highly defective parts of the particle. Due to a sudden temperature drop, the resultant oxide substitution phase is likely to be in an amorphous state. The observation of cone-shaped oxidation reaction in particles is analogous to the oxidation process associated with carbon nanotubes, being associated with highly imperfect tip areas.[21] In the case of carbon nanotubes, however, the product of the oxidation process is a volatile carbon oxide which cannot be observed directly attached to the nanotubes. Figure 9c illustrates another type of damage process induced by the shock waves which appears to be nondiffusion related. In this instance, many layers, particularly located at the outside part of the nanostructure, have fractured, while the inner layers seemingly remain intact, indicative of the partial destruction of this highly strained corner, as distinct from Figure 10a which appears to have fractured midbody.

B.7. Failure Mechanisms. The two types of damage mechanism identified suggest a locally heterogeneous distribution of stress and temperature during the shock process, leading to particle damage preferentially at stress-concentrated, highly energetic corner sites. When the temperature is high enough to allow for dynamic oxidation, the IF-WS_2 will become partly transformed to WO_x through diffusion, with the conversion process being constrained to the particle surface by a short period of time that the temperature remains high and by the limited diffusion distance of oxygen. As a result, the damage was enhanced at local faulted sites, resulting in the development of cone-shaped defects. This type of local conversion is considered to be a precursor for the mild or moderate structural failure of the IF nanostructures under the concurrent shock wave pressures.

When the applied shock pressures exceed the local IF-WS_2 or MoS_2 layer strengths, the layers break into smaller flakes, without the need for any local atomic diffusion. Depending to some extent on the localized defect conditions, it is considered that the nondiffusive direct structural damage becomes more significant at higher pressures. This can lead to severe destruction of an entire IF structure (e.g., Figure 10). At pressures up to 25 GPa, the direct structural destruction of the IF structures was limited, with only a few outer shell layers being broken and peeled off. For shock wave pressures above 30 GPa, as indicated by XRD and Raman analyses, the overall structural features of the IFs are much closer to those of their counterpart 2H platelet configurations, with direct structural damage becoming dominant, following the IF cage to 2H platelet transformation. Figure 9d shows a relatively spherical IF-MoS_2 particle suffering no obvious damage after exposure to a pressure of 24.6 GPa. For crucial industrial applications involving high pressures, perfectly shaped spherical IF nanoparticles are preferable for improved performance, being more resistive to conditions related to both the diffusive-controlled and direct damage failure mechanisms.

B.8. Oxide Core Effects. The role of the unconverted oxide cores sometimes contained within the nanoparticles is now considered. The inner WO_x cores are considered to support and strengthen the tube/particle mechanical properties. This supportive effect seems dominant under conditions of local hydrostatic pressure. However, for the case of dynamic pressure produced by shock waves, or for nonperiodic compression and shear stresses induced by tribological processes, the effect of the oxide core needs to be revaluated. Figure 10 shows HRTEM images of IF-WS_2 and MoS_2 nanoparticle cases, suggesting that "rigid" oxide cores act to accentuate the structural failure of the IFs. The residue of partly or fully deformed oxide cores was frequently observed during the investigation (Figure 10a−c); while hollow-caged structures tended to remain intact under similar shock wave conditions (Figure 10d). Figure 10a illustrates a nanoparticle with a rigid oxide core that had undergone a complete shattering in the midsection, rather than failing at the corners regions. In all these cases the oxide residues (Figure 10a−c) were present at the side of cages exposed to the shock wave front, indicating nonuniaxial process of rupture caused by the propagation of shock waves through the filled IF structures. Apparently, this rupture falls into the nondiffusive direct damage type of failure.

Structurally, the crystalline oxide cores differ from the outer sulfide layers, making the corresponding nanoparticle structure more rigid and less flexible under induced dynamic stress. Conversely, both hollow and filled IFs exhibit large interplanar spacing, are more able to respond elastically to absorb the induced shock wave pressures, eventually regaining more or

(21) Tsang, S. C.; Harris, P. J. F.; Green, M. L. H. *Nature* **1993**, *362*, 520.

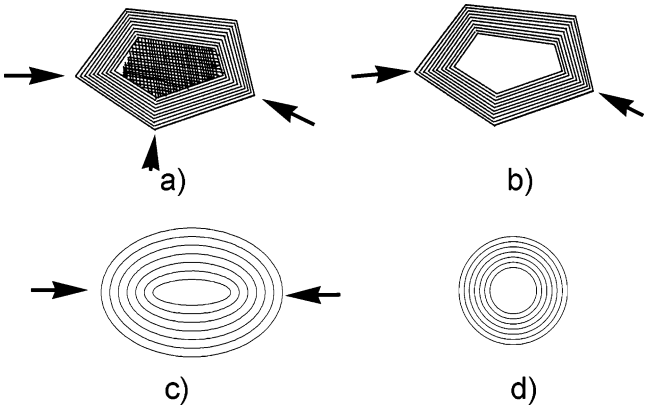

Figure 11. Schematic illustration of the likelihood damage of IFs under shock wave pressure: (a) a polyhedral IF-WS_2 nanoparticle filled with oxide core, may involve three types of destruction at both ends (diffusion-controlled + direct peeling off of layers) and at the midbody via direct breakage (arrowed); (b) an identical IF-WS_2 nanoparticle to that in (a) without any filling, may be damaged only at the ends (arrowed); (c) an olive-shaped IF-WS_2 particle, with much improved antishock behavior, may also be damaged at the ends (arrowed); (d) a smaller perfectly shaped spherical IF-WS_2 nanoparticle, expected to exhibit maximum shock-absorbing performance.

less their original layer separation and shape after pressure release simply via stress relaxation. For the case of more dynamic local pressure, the presence of a central oxide core acts to stiffen the nanoparticle, facilitating breakage of the cage from within. Accordingly, improved shock-absorbing properties of IFs must be accomplished by full conversion to perfect hollow crystalline IF cages.

In fact, a preliminary tribological study was also carried out with IF nanoparticles in which an oxide core was deliberately left (by noncomplete sulfidization). This study did not find any advantage for such filled nanoparticles compared with IF nanoparticles with empty cores (where the sulfidization reaction was completed).

Based on the above experimental data and mechanism discussion, we demonstrate the likelihood damage under shock waves using several model IF nanoparticles (Figure 11), taking into account the following factors: exterior geometry, inner filling, and overall dimensions. It is expected that the shock-absorbing property of these model IF nanoparticles, from Figure 11a−d, will be significantly increased by avoiding the two possible destructive mechanisms we have proposed. The perfectly shaped spherical, small model particle shown in Figure 11d is expecting to exhibit maximum antishock performance.

B.9. Comparison with Tribological Deformation Features. Tribologically tested IFs and postshock samples share many common features in terms of their structural failure. In a previous paper,[4] Rapoport et al summarized the failure of IF particles under friction and wear experiments with reference to ovoid-shaped deformation, radius of curvature change, external layer peeling, and structural splitting. The surface splintering features, as well as the ovoid-shaped elongated Ifs, are akin to the postshock samples examined here. At high load pressures during wear testing (420 N), most of the damage was caused by a peeling off of external layers.[22] In this context, the role of a central oxide core on the overall tribological performance of such nanostructures requires further comprehensive assessment. The temperatures in the present shock wave experiments are much higher than those involved in the tribological lubricating processes, but the latter tests are much longer than the shock wave experiments. Yet in both cases similar oxidation processes occurred. Therefore, the data presented here has wider importance for a diverse range of industrial applications of IF nanoparticles where dynamic pressures concomitant with high temperatures are involved, being not only limited to lubrication or shock wave absorption process.

Summary

To sum up, the present study focused on fresh and systematic experimental examinations of two types of postshock samples, IF-WS_2 and IF-MoS_2. These nanoparticles are currently in high industrial demand because of their superior lubricating performance as compared with that of their traditional 2H polytype platelet counterparts. The results show that the majority of IFs are capable of sustaining shock pressure up to 25 GPa, accompanied with very high concurrent temperature up to 1000 °C. When localized pressure and temperature are high, IFs may suffer destructions via two possible mechanisms, i.e., direct stresses-induced breakage failure and diffusion-controlled oxidation, separately or combined. The original IF geometry, i.e., the typical contour shape, the corner angle, the overall size and the filled oxide cores, has significant influences on their antishock behavior. Importantly, similar effects were found to be implicated in the tribological behavior of IF nanoparticles as well. The superb antishock or shock-absorbing property of IFs suggests they are valuable materials for many applications where dynamic pressures and high temperatures are involved.

Acknowledgment. We thank the EPSRC (U.K.), the Israel Science Foundation, and the Israeli Ministry of Science and Technology for financial support. We thank Mr. K. Dinsdale for XRD and TGA analysis. R.T. is the director of the Helen and Martin Kimmel Center for Nanoscale Science.

JA054715J

(22) Rapoport, L.; Leshchinsky, V.; Lapsker, I.; Volovik, Y.; Lvovsky, M.; Popovitz-Biro, R.; Feldman, Y.; Tenne, R. *Wear* **2003**, *255*, 785.